



# A unified framework for performance-based wind engineering of tall buildings in hurricane-prone regions based on lifetime intervention-cost estimation

Wei Cui, Luca Caracoglia \*

*Department of Civil and Environmental Engineering, Northeastern University, Boston, MA 02115, USA*



## ARTICLE INFO

### Article history:

Received 11 July 2017

Received in revised form 14 February 2018

Accepted 16 February 2018

Available online 26 March 2018

### Keywords:

Performance-based wind engineering

Tall building aerodynamics

Wind tunnel

Experimental load errors

Hurricane wind directionality

Lifetime intervention cost

## ABSTRACT

Accurate evaluation of structural performance is necessary in modern tall building design. In wind engineering, the current approach employed by researchers is the Monte-Carlo sampling method. Structural failure probability is calculated by combining structural fragility curves with the random variability of wind speed and direction, depending on local wind climate. In the hurricane-prone regions of the USA, wind climate and its effects on building response require accurate assessment of wind-induced structural performance.

This paper proposes a simulation framework for tall buildings that combines fragility analysis with local wind climate information to evaluate structural vulnerability. Hurricane wind climate information directly considers maximum wind speed, wind direction along with their correlation at hurricane landfall. Consequently, structural fragility surfaces will be generated, conditional on these two variables. This result will be used to examine lifetime intervention cost accumulation, associated with nonstructural damage on the building façade, and to determine an “optimal” wind-direction-dependent building orientation.

© 2018 Elsevier Ltd. All rights reserved.

## 1. Introduction

### 1.1. General context, literature review and statement of purpose

Tall buildings are the land-mark and center of human activities. They greatly influence local culture, economy and society. Therefore, accurate evaluation of structural performance under extreme winds is necessary. The designation performance-based design (PBD) has been originally coined and employed in seismic engineering over the past several years, as an alternative to the prescriptive design methods, based on the correspondence between earthquake recurrence intervals and performance levels [1]. The basic concept of PBD is to ensure that the structure satisfies a set of pre-defined performance requirements [2], when subjected to different hazard levels. Implementation of similar PBD-inspired methods has been recently considered in wind engineering and for various structures sensitive to wind-induced loads. The PBD is also attractive since it enables cost-effective design by assisting with the planning of maintenance in the aftermath of a catastrophic event.

Currently, the Monte-Carlo sampling method is used to calculate the probability of “structural failure” in a tall building at various wind speeds and to generate structural fragility curves, needed by PBD. The probability of structural failure, i.e., exceedance of a pre-selected limit-state threshold level, can be efficiently computed by repeating the random analysis  $N$  times (sample population size), since algorithmic complexity is not influenced by the number of uncertain or random quantities. Numerous studies have appeared in recent years to more rationally extend the PBD methodology to wind-load-sensitive structures (e.g., [3–10]). Literature review on PBD in the wind engineering field has also revealed the interest in the study of load effects on low-rise buildings [11–15], since damage and collapse are possible. Among the various contributions, the research groups from Notre Dame University and the University of Michigan have made notable advancements in the field of structural optimization, inspired by PBD concepts, applied to tall buildings under wind loads [16,17].

### 1.2. Performance-based wind engineering of tall buildings: Research opportunities and motivation

The research group from Northeastern University has examined several issues related to performance-based wind engineering (PBWE) for vibration-sensitive structures, such as long-span

\* Corresponding author at: Department of Civil and Environmental Engineering, Northeastern University, 400 Snell Engineering Center, 360 Huntington Avenue, Boston, MA 02115, USA.

E-mail address: [lucac@coe.neu.edu](mailto:lucac@coe.neu.edu) (L. Caracoglia).

bridges [18,19] and tall buildings [20–24]. Principal emphasis has been given to the simulation and analysis of lifetime intervention costs. The research has been inspired by seminal studies applying monetary loss analysis to study wind loads and performance of other structures (e.g., [25,26]) and, more generally, seismic engineering models [27]. Study activities have also been recently expanded through collaboration with another research unit from the University of Perugia, Italy (e.g., [28,29]).

However, the wind climate in hurricane-prone regions and its relationship with the building response still call for more accurate assessment of wind-induced structural response and more precise performance evaluation over the structural lifetime. The state-of-the-art structural performance analysis method against wind hazards, proposed in recent years by this group, is composed of three steps aiming to: (1) identify the most unfavorable wind direction, which predominantly contributes to the extreme wind load, either by wind tunnel test or through computational fluid dynamics; (2) construct the structural fragility curves at various wind speeds through numerical simulation; (3) incorporate the building's local wind climate data into the structural fragility analysis to evaluate structural failure probability. One of the main simplifications, partially ignored in previous studies, is the possibility of multi-directional winds with variable (or predominant) mean wind direction, which may positively or negatively affect the structural vulnerability and, consequently, the lifetime cost estimation. The important role of wind direction in relation to the PBD of buildings has in fact been noted in the engineering practice [30] and recently examined in more detail (e.g., [29]).

### 1.3. Main objectives and anticipated outcomes of the study

This study proposes a unified formulation and simulation framework for tall buildings that combines comprehensive fragility analysis and accounts for both variable wind speed and direction when evaluating structural vulnerability. Furthermore, hurricane wind climate information directly considers maximum wind speed, wind direction along with their correlation at hurricane landfall. On one side, wind climate information will consider the correlation between reference wind speed and wind direction to construct the joint probability density function between these two variables and to quantify hazard intensity. On the other hand, structural fragility surfaces, conditional on these two variables, will be generated. This result will be used to investigate structural performance, to examine lifetime intervention costs accumulation due to nonstructural damage on the façade of a reference tall building and to determine an optimal wind-direction-dependent building orientation.

## 2. Background theory

### 2.1. Davenport's wind loading chain and its relationship to performance-based wind engineering (PBWE)

In 1961, Professor Alan G. Davenport established the theoretical fundamentals of structural analysis for wind engineering [31]. According to this approach, the wind-induced structural response of a tall building can be determined in the frequency domain through the combination of local wind climatology, local wind exposure and topography, structural aerodynamic characteristics, governed by building shape, and structural dynamic properties. This theory leads to the determination of the power spectral density (PSD) of the generalized turbulence-induced dynamic forces and the structural response [33,34]. Currently, this approach is referred to as the "Davenport Chain" [32].

One of the key steps of the PBWE is the evaluation of the probability that either a system or one of its sub-components reaches or exceeds a given limit state or "failure" probability conditional on the hazard intensity, such as the mean wind speed at a reference elevation. For serviceability limit states, which are usually predominant in the wind-resistant design of a tall building, a linear elastic structural model is adequate [35] and the standard frequency domain random vibration analysis of the Davenport Chain can be used [35–38]. On the basis of this concept, designers or owners can make a decision through appropriate decision variables (DVs) [3]. For example, Ciampoli and Pertini [3] presented a general framework to evaluate the structural risk as the probability of exceeding a prescribed threshold level of the relevant DV, described as:

$$G(DV) = \int \dots \int G(DV|DM)f(DM|EDP)f(EDP|IM, IP, SP)f(IP|IM, SP) \\ \times f(IM)f(SP)dDMdEDPdIMdIPdSP \quad (1)$$

A more detailed description of the variables can be found in [3] (IM: intensity measures, SP: Structural Parameters, IP: interaction parameters, EDP: engineering demand parameter, DM: damage measure). In most current PBWE evaluation methods, especially those for tall buildings, the measure of the wind hazard intensity only includes the extreme value of the wind speed. Wind direction is partially ignored in the PBWE analysis process, even though it is important [30] since aerodynamic forces and vortex shedding effects can drastically change with wind direction. Moreover, the prevailing wind direction at a specific location is not "uniformly" distributed, especially in the presence of tropical winds [39]. Therefore, it is necessary to correctly include the wind direction into PBWE analysis (e.g., [29]).

## 3. Framework description

### 3.1. Fundamentals, assumptions and description of the framework "modules"

The general procedure for PBD is schematically presented in Eq. (1). However, some steps are not directly applicable to wind engineering. For example, the damage analysis [ $f(DM|EDP)$ ] is associated with individual structural components, such as columns, beams, etc. Characterization of these components requires analysis of materials and mechanics. This task has not been considered but can be readily included in future work, e.g., following work carried out for reinforced-concrete buildings [40]. Furthermore, damage-induced monetary loss analysis [ $f(DV|DM)$ ] at the structural element level after the occurrence of the hazard is related to engineering economics and is not discussed herein.

Aiming to build a unified performance-based wind engineering formulation, this study will focus on the first four parts described in Eq. (1): the hazard analysis  $f(IM)$ , the structural parameter analysis  $f(SP)$ , the aerodynamic analysis  $f(IP|SP, IM)$  and the structural response analysis  $f(EDP|SP, IM, IP)$ . Monetary loss analysis is considered at the cumulative structural level only (e.g., [24]). Damage produced by structural vibration on the building façade is predominantly considered, as it is often observed on the façade of tall buildings. Other damage categories are not included but may be considered in future investigations. Supplementary discussion on the limit state selection is presented in a later section (Section 4.3). Moreover, the assumption  $f(DM|EDP) = 1$  is used in this paper; it should be noted that this assumption may cause non-conservative estimation of damage probability in the case of hurricane winds, since the damage is examined only for the worst-case scenario and does not consider the possibility of additional

wind-induced damage, as the wind speed and direction change during the storm.

In the remaining sub-sections of this part, the basic modules of the PBWE framework will be presented.

### 3.2. Hurricane simulation and characterization of site winds

#### 3.2.1. Analysis of gradient wind speed and direction

The prediction of wind hazards such as hurricanes is a sub-field of meteorology. Currently, two methods are predominantly used to analyze wind hazards for structures. The first method directly employs historical records of wind speeds (e.g., [19,24]), reliable if wind data sets are available at weather stations [41]. Nevertheless, because weather recording is a continuous process, historical data can be insufficient as they may include a mixture of distinct weather events, such as hurricanes, thunderstorms and tornadoes [42]. Therefore, a second method has been considered. This second method, originally proposed by Vickery et al. [43], utilizes a set of historical hurricane records to identify the main patterns of the wind hazard and to generate synthetic (hurricane) wind events. It is reliable since it can be validated using the historical records of hurricanes. In this study, Vickery's method [44,43] is employed to build the joint probability distribution of maximum wind speed and wind direction at hurricane landfall. Since numerical implementation was part of a previous study [45], the main aspects of the method are only summarized.

The basic idea of the synthetic simulation approach [43] is the tracking of  $c_i$  or hurricane translation speed,  $\theta_{h,i}$  or hurricane heading (direction) and  $I_i$  hurricane intensity (related to barometric pressure reduction inside the hurricane eye  $\Delta p$  [43]). Three empirical difference equations, numerically solved at each discrete time step  $i$  (every six hours), are used to predict  $c_i$ ,  $\theta_{h,i}$  and  $I_i$ . The coefficients of the model equations are calibrated by regression using the historical database "HurDat" [46]. The hurricane gradient wind field at maximum intensification (hurricane landfall) is later reconstructed from  $c_i$ ,  $\theta_{h,i}$  and  $I_i$ : the gradient wind speed ( $V_g$ ) can be found from the vector sum of a rotational component ( $V_R$ , cyclostormic vortex model) and a translational component ( $V_T = c$ , hurricane translation) in accordance with Georgiou's model [47]:

$$V_g = \frac{1}{2}(c \sin \alpha_T - f_c r) + \sqrt{\frac{1}{4}(c \sin \alpha_T - f_c r)^2 + \frac{100B_H \Delta p}{\rho} \left(\frac{R_{\max}}{r}\right)^{B_H} \exp\left[-\left(\frac{R_{\max}}{r}\right)^{B_H}\right]} \quad (2)$$

In Eq. (2)  $c$  is the magnitude of the translation speed at landfall;  $f_c$  is the Coriolis parameter;  $\alpha_T$  is the relative angle between hurricane heading and radial position;  $B_H$  is the Holland parameter;  $\Delta p$  is the barometric pressure reduction;  $R_{\max}$  is the radial distance from the hurricane eye corresponding to maximum wind intensities [48]. This procedure is schematically presented in Fig. 3 of [45].

#### 3.2.2. Joint probability density function of gradient wind speed and direction

Reference wind speeds and wind directions at specific locations along the eastern US coastline can be generated using 20,000 years of synthetic hurricane simulation [45], as outlined in Section 3.2.1. The hurricane wind-speed marginal probability distribution can usually be modeled by a Weibull distribution. Nevertheless, to the authors' knowledge the joint probability density function (PDF) of wind speed and direction has never been examined before. The joint PDF of wind speed and direction can be determined by angular-linear distribution [49,50]:

$$f_{V_g, \Theta}(v_g, \theta) = 2\pi g(\zeta_g) f_{V_g}(v_g) f_\Theta(\theta); \quad 0 \leq \theta \leq 2\pi; \quad 0 < v_g < \infty \quad (3)$$

Following the work by Carta et al. [50], the gradient wind speed PDF  $f_{V_g}(v_g)$  is modeled as a singly Truncated distribution, derived from the Normal and Weibull mixture distribution (TNW-PDF) described below [49]:

$$f_{V_g} = \frac{\omega_0}{I(\phi_1, \phi_2)} Z(v_g, \phi_1, \phi_2) + (1 - \omega_0) \frac{a_V v_g^{(a_V)-1}}{(b_V)^{a_V}} \exp\left[-\left(\frac{v_g}{b_V}\right)^{a_V}\right] \quad (4)$$

where  $Z(v, \phi_1, \phi_2)$  and  $I(\phi_1, \phi_2)$  are functions given below [49,50]:

$$Z(v_g, \phi_1, \phi_2) = \frac{1}{\sqrt{2\pi}} \exp\left[-\left(\frac{(v_g - \phi_1)^2}{2\phi_2^2}\right)\right] \quad (5)$$

$$I(\phi_1, \phi_2) = \frac{1}{\phi_2} \int_0^\infty Z(v_g, \phi_1, \phi_2) dv_g \quad (6)$$

For the wind direction PDF,  $f_\Theta(\theta)$ , a mixture of von Mises distribution models can be used [49,50]:

$$f_\Theta(\theta) = \sum_{j=1}^{N_m} \frac{\omega_j}{2\pi I_0(\kappa_j) \exp\left[\kappa_j \cos(\theta - \mu_j)\right]]; \quad 0 \leq \theta \leq 2\pi \quad (7)$$

In Eq. (7),  $I_0(\kappa_j)$  is the modified Bessel function of the first kind; quantities  $\kappa_j \geq 0$  and  $0 \leq \mu_j < 2\pi$  are parameters [49,50]; the weighting factors  $\omega_j$  should satisfy the following relationships:

$$0 \leq \omega_j \leq 1; \quad \sum_{j=1}^{N_m} \omega_j = 1 \quad (8)$$

In Eq. (3), the  $g(\cdot)$  is the PDF of the "circular variable"  $\zeta_g$ , given by:

$$\zeta_g = 2\pi[F_{V_g}(v_g) - F_\Theta(\theta)] \quad (9)$$

where  $F_{V_g}(v_g)$  and  $F_\Theta(\theta)$  respectively are the cumulative distribution functions (CDFs) of wind speed  $v_g$  and wind direction  $\theta$  at a reference height. The values of  $\zeta_g$  obtained from the equation above, which are smaller than zero, are recalculated as  $\zeta_g = \zeta_g + 2\pi$  to get  $0 \leq \zeta_g \leq 2\pi$ . Traditionally, a mixture of von Mises distributions is also used to model the PDF of the circular variable  $\zeta_g$  [50].

Following the procedure described in [50], the wind hazard probabilistic model  $f_{V_g, \Theta}(v_g, \theta)$  can be built for any specific area along the eastern US coastline and incorporated in the hazard analysis part ( $f(IM)$ ) of the PBWE framework. The model coefficients  $\omega_j$ ,  $a_V$ ,  $b_V$ ,  $\kappa_j$  and  $\mu_j$  can be calibrated by maximum likelihood estimation method. In the case of other non-hurricane wind hazards, the same approach may be used to construct the joint PDF of  $v_g$  and  $\theta$ . In any case, since hurricanes are the dominating wind hazard in the eastern US coastal areas and damage induced by synoptic winds on tall buildings is of secondary importance in these regions of the United States [24], hurricane-induced damage can exclusively be considered in the accumulation of intervention cost.

### 3.3. Building aerodynamics and structural dynamic response

#### 3.3.1. Description of the benchmark building application

In order to demonstrate the feasibility of the proposed framework, one application example is used. The building model reflects the properties of the CAARC benchmark building. The main features are briefly described in this section.

The CAARC building was first proposed as a standard building model for comparison among experimental wind tunnel techniques and laboratories by the Commonwealth Advisory Aeronautical Research Council (CAARC) [51]. Numerous studies have used the CAARC building as a reference for validation of several

aerodynamic analysis methods. In the 1980's several studies were conducted to examine aerodynamic load variability and the influence of the geometric scale of the CAARC model on the wind load results (e.g., [52–54]). Later investigations [55,56] evaluated the interference effects between two identical CAARC building models by wind tunnel tests. In recent years, the CAARC building model has also been used to explore computational fluid dynamics (CFD) in wind engineering; several researchers (e.g., [57–59]) employed numerical simulations to determine the wind loads and validated their results against wind tunnel experimental data.

This building can be modeled as a slender prismatic cantilever structure with a rectangular floor-plan section. The structure is symmetrical about local axes of lateral bending (i.e., local coordinate system designated by  $x, y$  in Fig. 1b). The mean wind direction, corresponding to the relative mean-wind incidence angle  $\Psi = 0$ , coincides with the direction  $x$  in Fig. 1b.

### 3.3.2. Experimental aerodynamic loads: Variability and errors

Similar to uncertain wind speed and wind direction, the parameters describing structural properties and wind loads applied to a tall building are also random due to the unavoidable observational and identification errors. Researchers suggest that, for example, every parameter should be independently examined at each step of the Davenport Chain: uncertainties arising from incomplete knowledge of the surface pressures in a wind tunnel experiment (e.g., [7]) and various error sources related to the analysis of the aerodynamic loads [18,24].

Acquisition of a large load data set is needed to identify the uncertain parameters. Moreover, the use of several uncertain parameters and the presence of coupled structural-modal coordinates induce a drastic increase in the computing time for calculating the generalized modal forces [60] and prevents from the implementation of rigorous methods for aeroelastic uncertainty propagation, such as stochastic calculus [61]. For these reasons, universal implementation of PBWE is still challenging. To overcome these limitations and recognizing the key role of the aerodynamic loads, the present formulation proposes a set of model equations to represent the power spectral density (PSD) functions of the generalized along-wind force  $S_{Q_x Q_x}$ , cross-wind force  $S_{Q_y Q_y}$ , and torque  $S_{TT}$ , associated with the fundamental lateral building modes. Three model equations are introduced to describe  $S_{Q_x Q_x}$ ,  $S_{Q_y Q_y}$  and  $S_{TT}$ . The equation below, valid for cross-wind generalized load, is exclusively presented as an example.

$$\frac{nS_{Q_y Q_y}(n)}{\left(\frac{1}{2}\rho\bar{U}^2(h)Dh^2\right)^2} = \frac{a_L f}{1 + b_L f^{c_L}} + d_L f^2 \exp\left[-\left(\frac{f - e_L}{f_L}\right)^2\right] \quad (10)$$

In the previous equation  $\rho$  is the air density,  $h$  is the total building height,  $D$  is a reference width of the building section,  $n$  is the frequency (Hz);  $f$  is a normalized frequency, which is defined as  $f = nD/\bar{U}(h)$ ; the reference mean wind speed  $\bar{U}(h)$  is the ten-minute average wind speed, evaluated at the building roof top  $z = h$  in open-terrain exposure category (coastal areas);  $a_L, b_L, c_L, d_L, e_L, f_L$  are empirical parameters to be determined along with their randomness. The previous equation and other equivalent formulas [62] provide the directional solution to the aerodynamic loads, since they can be estimated for various mean-wind incidence angles ( $\Psi$ ) relative to a reference horizontal axis of the building's local coordinate system ( $x$ ). Generalized wind loads can in fact be found from a wind tunnel test, i.e., measured as base bending moments and base torque by a high-frequency force balance (HFFB) on a scaled model of a tall building (e.g., [63,64]).

In order to examine the feasibility of the experimental approach along with the analysis of the error sources, specific experiments have been conducted in the Northeastern University's small-scale wind tunnel [65]. The along-wind base bending moment, cross-wind base bending moment and base torque of a 1:750-scale model of the CAARC building were acquired by HFFB, considering nine different  $\Psi$  angles. The main results are presented in this sub-section; more details may be found in previous studies [65,62].

Fig. 2 illustrates an example of normalized PSD curves of the base bending moments for the cross-wind loads and relative mean-wind incidence angle  $\Psi = 0^\circ$ . Each plot is the result of one wind tunnel test, derived from Eq. (10); the horizontal axis is the reduced frequency  $f = nD/\bar{U}(h)$ . The presence of a "cluster" of plots confirms that the shape of each PSD function is similar but variability exists due to random imperfections in the measurements, sensor and digital data communication disturbances. Dispersion is larger at  $f > 0.3$  because of the particular signal post-processing procedure [65], employed to extract each PSD curve. Experimental error is not negligible in Fig. 2. It can be assimilated by allowing the parameters in the formula of Eq. (10) to vary randomly. Repetition of the experiments several times under the same laboratory conditions and the same  $\Psi$  enables the examination of the errors. Repeated experiments also allow to determine the probability distributions of the parameters along with their mutual correlation. After suitable verification and validation, the random parameters

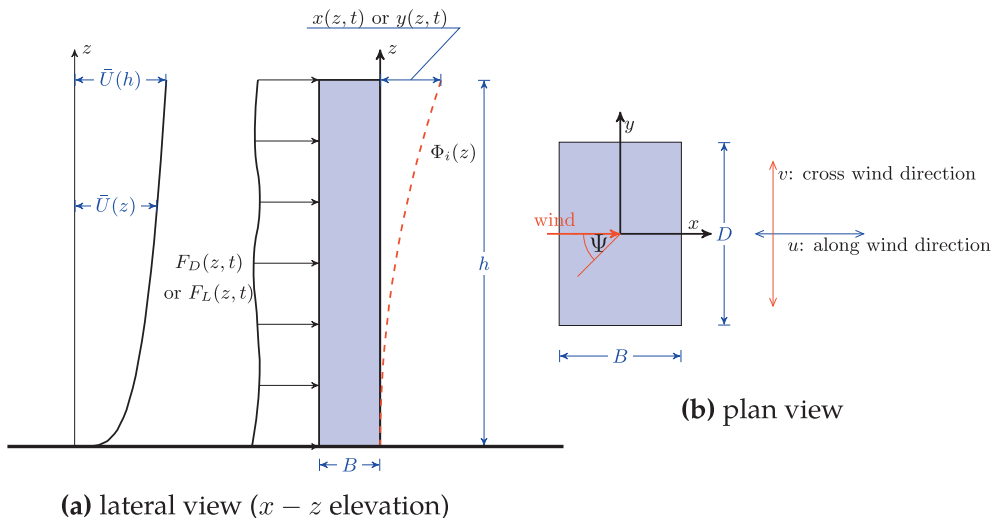


**Fig. 1.** Schematic of CAARC tall building aerodynamics [51] and wind-load directionality ( $\Psi$  is the relative mean-wind direction angle).

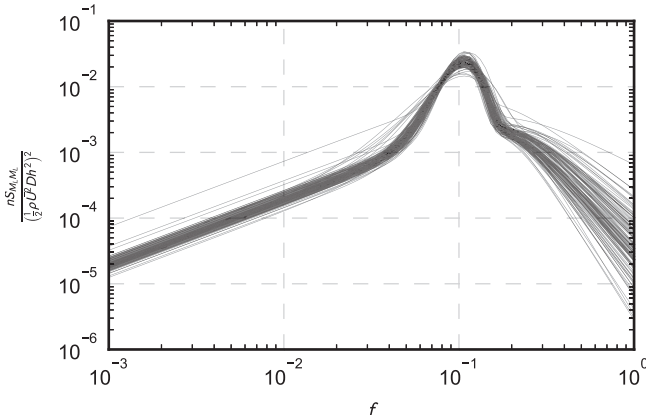


**Fig. 2.** CAARC building model: repeated realizations (variability) of the experimental wind force PSD for reference relative mean-wind incidence angle  $\Psi = 0^\circ$ : cross-wind base bending moment  $S_{Q_y Q_y}$ .

can be synthetically re-generated to reconstruct the generalized PSD of the wind loading from formulas such as Eq. (10) and consequently be used for Monte-Carlo analysis. Details are discussed in [62], for both  $S_{Q_x Q_x}$ ,  $S_{Q_y Q_y}$  and  $S_{TT}$ .

The previous results can be presented in the form of  $f(IP|IM)$ , i.e., the second part of the PBWE framework. The novel contribution of this approach is the error quantification of the parameters related to vortex-shedding (e.g.,  $d_L$ ,  $e_L$  and  $f_L$  in Eq. (10)), which are usually not considered in the current wind engineering research and practice. Finally, other randomness sources, such as the structural dynamic properties  $B$  (width),  $D$  (depth),  $h$  (height) and the aerodynamic parameters per unit height (drag  $C_D$ , lift  $C_L$  and moment  $C_M$ ) can readily be included along with the PSD model equations (e.g., Eq. (10)) to derive  $f(SP)$  in accordance with the Davenport Chain.

### 3.3.3. Tall building response

The combination of the joint PDF of the reference wind speed and direction in the context of a multi-directional aerodynamic force analysis requires an advanced structural aerodynamic response calculation method. For example, not only does a multi-directional wind analysis cause multi-directional wind loads on the full-scale structure but it also leads to complex dynamic motion in the presence of coupled modal coordinates and non-uniplanar modes shapes. The paper [66] proposes a “universal” analytical approach for the three-directional (3D) response, induced by multi-directional winds and coupled structural response. It is possible to further generalize the approach [66] in the context of PBWE. The fundamental generalized dynamic scalar modal equation, describing the response of mode  $j$  in the frequency domain, becomes:

$$\left\{ s_{jj} + ifc_{jj} + \frac{8m_j\pi^2}{\rho D^4 h} [f_j^2 + 2\xi_j f_j if - f_j^2] \right\} \hat{\chi}_j(f) + \sum_{k=1, k \neq j}^N [s_{jk} + ifc_{jk}] \hat{\chi}_k(f) = \hat{q}_j \quad (11)$$

In the previous equation  $\hat{q}_j$  is the dimensionless generalized buffeting force for the  $j$ -th mode;  $c_{jk}$  is a dimensionless generalized aerodynamic damping force;  $s_{jk}$  is a dimensionless generalized aerodynamic stiffness force and  $i = \sqrt{-1}$ . The formula above is dimensionless. The quantity  $f$  is the dimensionless frequency, defined earlier, and  $\hat{\chi}$  is the generalized structural response vector in the modal coordinates; the “hat” symbol designates Fourier

transformation according to frequency variable  $f$ . As an example, the generalized loads is:

$$\begin{aligned} \hat{q}_j &= \int_0^1 \Delta(\zeta) [\phi_{xj} \quad \phi_{yj} \quad \phi_{pj}] \begin{bmatrix} \cos \Psi & -\sin \Psi & 0 \\ \sin \Psi & \cos \Psi & 0 \\ 0 & 0 & 1 \end{bmatrix} \times \begin{bmatrix} 2C_D(\Psi) & C'_D(\Psi) - C_L(\Psi) \\ 2C_L(\Psi) & C'_L(\Psi) + C_D(\Psi) \\ 2C_M(\Psi) & C'_M(\Psi) \end{bmatrix} \begin{Bmatrix} \hat{\mu}(\zeta, f) \\ \hat{v}(\zeta, f) \end{Bmatrix} d\zeta \end{aligned} \quad (12)$$

Similar expressions can be determined for  $c_{jk}$  and  $s_{jk}$  (not shown for the sake of brevity). In the previous equation  $\zeta$  is a dimensionless vertical coordinate with  $z = \zeta h$ ;  $\mu = u/\bar{U}(h)$  and  $v = v/\bar{U}(h)$  are dimensionless turbulence components; the prime apostrophe indicates the derivative with respect to the mean-wind incidence angle. By assembling all the generalized motions in each mode of interest, the coupled structural response can be derived in matrix format [66].

When the structural modes shapes of mode  $j$  ( $\phi_{xj}, \phi_{yj}, \phi_{pj}$ ) are linearly increasing functions from the ground floor to the top floor and modes are uni-planar, the generalized forces  $\hat{q}_j$  of the fundamental modes can be replaced by the HFFB base bending moments and base torque (Section 3.3.2). The matrix  $\mathbf{S}_{Q,Q_i}$  below designates the generalized force PSD, obtained experimentally by considering three uncoupled modal coordinates and mode shapes linearly varying with height:

$$\mathbf{S}_{Q,Q_i} = \iint_0^1 \Delta(\zeta_1) \Phi_l(\zeta_1) C^* \begin{bmatrix} S_{\mu\mu}(\zeta_1, \zeta_2) \\ S_{vv}(\zeta_1, \zeta_2) \end{bmatrix} C^{*,T} \Phi_l^T(\zeta_1) \Delta(\zeta_2) d\zeta_1 d\zeta_2 \quad (13)$$

$$\Phi_l(\zeta) = \begin{bmatrix} 1 & 0 & 0 \\ 0 & 1 & 0 \\ 0 & 0 & 1 \end{bmatrix} \zeta \quad (14)$$

For a building structure with complex 3D mode shapes,  $\Phi_l(\zeta)$  must be modified to allow using the HFFB test results with the structural response analysis. The PSD matrix of the aerodynamic loads is derived from the previous equation as  $\mathbf{S}_{QQ} = \Lambda \Xi \mathbf{S}_{Q,Q_i} \Xi^T \Lambda^T$ ;  $\Lambda = [\lambda_1 \quad \lambda_2 \quad \dots \quad \lambda_N]^T$  is the modification matrix composed of  $N$  modification vectors,  $\lambda_j = [\beta_{xj} \quad \beta_{yj} \quad \beta_{pj}]$ , one for each mode. In each  $\lambda_j$ , the quantities  $\beta_{xj}, \beta_{yj}$  and  $\beta_{pj}$  are correction factors for nonlinear mode shapes [67]. The quantity  $\Xi$  is a rotation matrix that projects the HFFB force matrix from along-wind, cross-wind coordinates to the structure's local coordinates ( $x, y$ , principal lateral bending planes) and depends on the mean-wind incidence angle  $\Psi$ . Finally, the PSD matrix of the generalized structural response can be calculated, from the HFFB results and  $\mathbf{S}_{QQ}$ , as  $\mathbf{S}_{xx} = \mathbf{H} \mathbf{S}_{QQ} \mathbf{H}^{*,T}$ . The quantity  $\mathbf{H}^{*,T}$  is the conjugate transpose of  $\mathbf{H}$ , with transfer function matrix  $\mathbf{H}$  linking the force vector  $\mathbf{Q}$  to the generalized response vector  $\mathbf{X} = [\chi_1, \chi_2, \dots, \chi_N]^T$ . Derivation of  $\mathbf{H}$  is omitted for the sake of conciseness.

Through the equations above, the HFFB test results along with the experimental errors (Section 3.3.2) can directly be related to structural response uncertainty. The randomness of the parameters in Eq. (10) and similar formulas can be brought into the generalized structural response spectrum  $\mathbf{S}_{xx}$ , which can be re-converted to local physical building coordinates to enable the structural fragility analysis at various reference mean wind speeds and wind directions.

### 3.3.4. Verification and validation of the CAARC model and results

Prior to the derivation of the fragility simulation model, verification and validation of the approach discussed in this section is necessary. Fig. 3 illustrates the results obtained for the CAARC

benchmark building at mean-wind incidence angle  $\Psi = 0$ . Results are based on the numerical model, described in Section 3.3.3, combined with experimental data from the Northeastern University's wind tunnel. Additional information and more details are presented in [24]. In the figure the responses in the along-wind and cross-wind directions are compared to aeroelastic wind tunnel results derived from [51]. Both RMS (root mean square,  $\sigma_x$  and  $\sigma_y$ ) and mean responses ( $\bar{X}$ ) are examined. The mode shape functions, used in this verification example, are linear; inter-modal coupling is neglected to comply with the hypotheses used in [51]. Excellent correspondence among the various curves may be noted. This result confirms the validity of the proposed formulation and further verifies the applicability of the proposed numerical/experimental approach.

### 3.4. Probability-based life-cycle intervention cost estimation

#### 3.4.1. Structural fragility surfaces for multi-directional winds

For multi-directional wind loads on structures, the mean wind speed at the reference height  $z = h$ ,  $\bar{U}(h)$ , and mean wind direction  $\bar{\theta}$  should be considered as the input variables of the fragility function [19]:

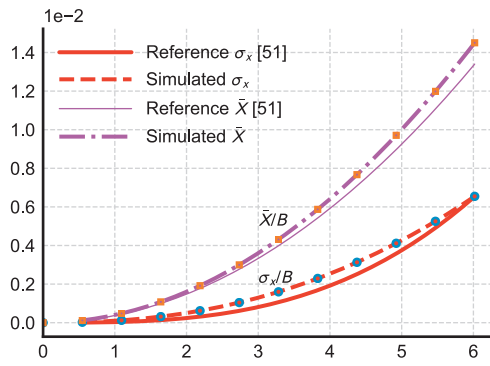
$$f_l(u_h, \theta) = P(EDP_l \leq d_l | \bar{U}(h) = u_h, \bar{\theta} = \theta) \quad (15)$$

The fragility function described by Eq. (15) is a fragility surface, which considers the conditional failure probability for various combinations of reference wind speed and wind direction. Overall, the structural response uncertainty calculated from Section 3.3.3, which is included in Eq. (15), forms the structural analysis module  $f(EDP|SP, IP)$  of the proposed PBWE framework.

#### 3.4.2. Structural damage probability and lifetime intervention cost estimation

After integrating the wind climate information [ $f(IM)$ ] with the structural analysis ( $f(EDP|SP, IP)$ ), the structural failure probability can be derived for the specific duration, for example, one year. Correspondingly, the wind climate function  $f(IM)$  should represent the joint probability distribution of wind speed and wind direction during any one-year period (e.g., yearly maxima [24]). Alternatively, the joint probability distribution of a single hazard event along with the frequency of events for each year can be used. Because the simulated hurricane wind speeds and wind directions are based on the synthetic simulation of each event, the latter method is preferable and is employed in this study.

The structural damage probability associated with limit state  $l$  in one hurricane event is calculated as:



(a) Along-wind response

$$P_{l,\text{event}}(\Omega) = \int_0^{2\pi} \int_0^{\infty} f_{u_h, \Theta}(u_h, \theta) f_l(u_h, \theta + \Omega) du_h d\theta \quad (16)$$

In the previous equation, one extra variable  $\Omega$  (Fig. 4) is introduced to consider the building orientation (i.e., the angle between the direction of  $x$  local coordinate axis and the North direction). The angle  $\Omega$  is used in conjunction with the reference direction for hurricane tracking and synthetic generation. Therefore, the quantity  $P_{l,\text{event}}(\Omega)$  evaluates the structural failure probability accounting for variable building orientation.

Thus the damage probability corresponding to limit state  $l$  in a one-year period at time  $t$  ( $t = \{1, 2, \dots, N_s\}$  years) is:

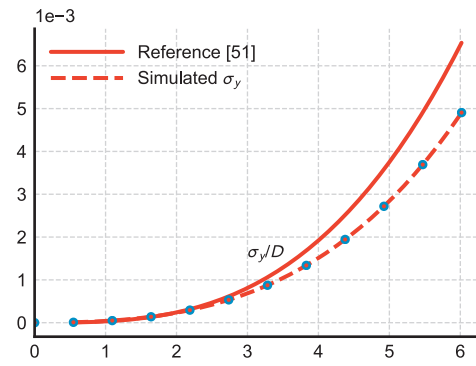
$$P_l(t) = 1 - (1 - P_{l,\text{event}})^{N_h(t)} \quad (17)$$

where  $N_h(t)$  is the random number modeling the hurricane event frequency for one specific location along the eastern US coastline at time  $t$  (year), and  $P_l(t)$  is the annual structural failure probability with  $N_h$  hurricane events observed within this year  $t$ .

The algorithm for lifetime intervention cost analysis employs the fragility analysis result (from the previous sub-section) to predict damage-induced monetary losses over the structural lifetime (time  $t_{N_s}$  with unit of years). When estimating the lifetime intervention cost for a building structure, it is convenient to express the cost model in terms relative intervention costs  $C_{M,E}$ , i.e., the expected value of maintenance and repair costs normalized with respect to the initial construction cost  $C_0$  [19]:

$$C_{M,E} = E \left[ \frac{C(t_{N_s}) - C_0}{C_0} \right] = E \left[ \sum_{i=1}^{N_s} \sum_{l=1}^{k_s} \epsilon_l e^{-\lambda t_i} P_l(t_i) \right] \quad (18)$$

In the previous equation,  $E[\cdot]$  denotes expected value;  $i$  is an integer number indexing the occurrence of the hazards over the structural life;  $t_i$  is the  $i$ th time (year) when the hazard occurs;  $N_s$  is the total structural lifetime in years;  $l$  is the index used to designate the different limit states;  $k_s$  is the total number of limit states considered. The total cost  $C(t_{N_s})$  is a function of time  $t_{N_s}$ ;  $\epsilon_l = C_l/C_0$  is the ratio between the intervention cost  $C_l$  in present dollar value of the  $l$ th limit state being reached at time  $t_i$  and the construction cost  $C_0$ ;  $e^{-\lambda t_i}$  includes the discount factor of  $C_l$  ( $\epsilon_l$ ) at time  $t_i$ ;  $\lambda$  is a constant discount rate per year;  $P_l$  is the probability of the  $l$ -th limit state being reached. The previous equation implies that the structure is repaired immediately after damage has occurred. Moreover, it does not include scheduled maintenance costs and structural aging of cladding and components, since they do not depend on the wind-induced damage occurrence and orientation  $\Omega$ . Consequently, they can be excluded from the optimization procedure.



(b) Cross-wind response

Fig. 3. Comparison between simulated response at the roof-top of the CAARC building and wind tunnel test results, reproduced from [51].

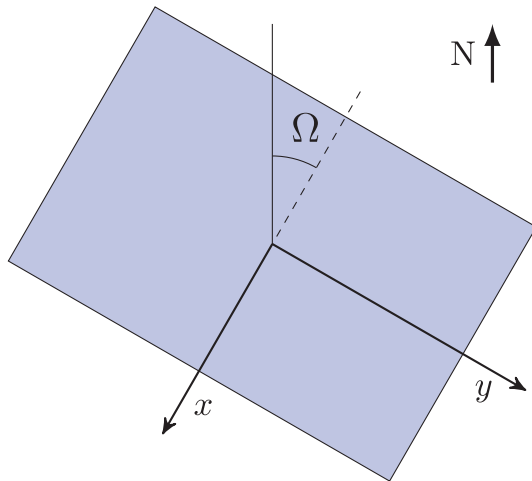


**Fig. 4.** Schematic of building's orientation (top view).

### 3.5. Summary: Flowchart of the simulation framework

The Monte-Carlo simulation method, combining the approaches described in the previous sub-sections, can be used during each step of the probabilistic analysis from wind climate to structural parameter estimation.

The whole framework is illustrated in Fig. 5. The framework can be divided into three parts or “modules”: (1) long-term synthetic hurricane simulation is used to predict hurricane arrival rate and intensity; (2) wind tunnel test are carried out at various  $\Psi$  angles to identify PSD of wind loads and their uncertainty; (3) fragility surfaces, constructed for various wind speeds and directions, are combined with the hurricane model results to evaluate structural performance and lifetime intervention cost.

## 4. Numerical results

### 4.1. Site wind modeling results

The CAARC benchmark building is assumed to be located in Miami, Florida, an area severely impacted by hurricanes along the eastern US coastline. Using the simulation method described in Section 3.2.1 20000 years of synthetic hurricane results are collected [68]; there are 20019 hurricane events recorded at this location (i.e., within the nearby influence region). For each record, the maximum wind speed and corresponding wind direction derived from the hurricane pressure field at hurricane landfall, are extracted. The raw wind climate data are used to determine the joint probability distribution  $f_{V_g,\Theta}(v_g, \theta)$  of the gradient wind.

As mentioned in Section 3.2.2, the marginal distribution of the wind speed can be simulated by a Weibull distribution in Eq. (19) below instead of Eq. (4), if hurricane events are exclusively considered:

$$f_{V_g}(v_g) = \frac{a_V v_g^{a_V - 1}}{(b_V)^{a_V}} \exp\left[-\left(\frac{v_g}{b_V}\right)^{a_V}\right] \quad (19)$$

Fig. 6 illustrates the empirical histogram of the gradient wind speed found from the 20019 hurricane events and the corresponding PDF obtained from the Weibull model. Good correspondence between the raw data and the model confirms that the Weibull model adequately replicates the wind speed distribution.

Fig. 7a illustrates the angular histogram of the reference wind direction and the corresponding PDF model, fitted using the function in Eq. (7). Examination of the histogram suggests that there are two local peaks in the distribution of the wind direction, thus the parameter  $N_m$  in Eq. (7) is set to 2. The empirical histogram and PDF model match very well, demonstrating that the von Mises model adequately represents the wind direction distribution. Similarly, the variable  $\zeta_g$ , which identifies the angular difference between the CDF of the wind speed and wind direction data pair [Eq. (9)], is shown in Fig. 7b. The graph demonstrates that the von Mises model also satisfactorily simulates the  $\zeta_g$  distribution.

The multiplication among the functions  $f_{V_g}(v_g)$ ,  $f_\Theta(\theta)$  and  $g(\zeta_g)$  leads to the joint PDF of the gradient wind speed and wind direction  $f_{V_g,\Theta}(v_g, \theta)$ . The PDF of  $f_{V_g,\Theta}(v_g, \theta)$  is plotted in Fig. 8. This result can be used for the structural damage probability analysis in the next section after suitable re-scaling of the  $v_g$  variable, the gradient wind speed, to the wind speed at building roof-top  $u_h = \bar{U}(h)$  [69]. This variable transformation leads to  $f_{u_h,\Theta}(u_h, \theta)$ , needed for the fragility analysis in Eq. (16).

### 4.2. Structural fragility surfaces accounting for wind tunnel experimental error

In order to demonstrate the full applicability of Eq. (11) and contrary to the original model [51], the matrix function describing the structural mode shapes in terms of the coordinate  $\zeta$  is assumed as:

$$\Phi(\zeta) = \begin{bmatrix} 1 & 0 & 0.1 \\ 0 & 1 & 0 \\ 0.05 & 0 & 1 \end{bmatrix} \zeta \quad (20)$$

The lateral translation response along the  $x$  direction (local building axes) is coupled with the torsional motion; the translation motion along the  $y$  direction is independent.

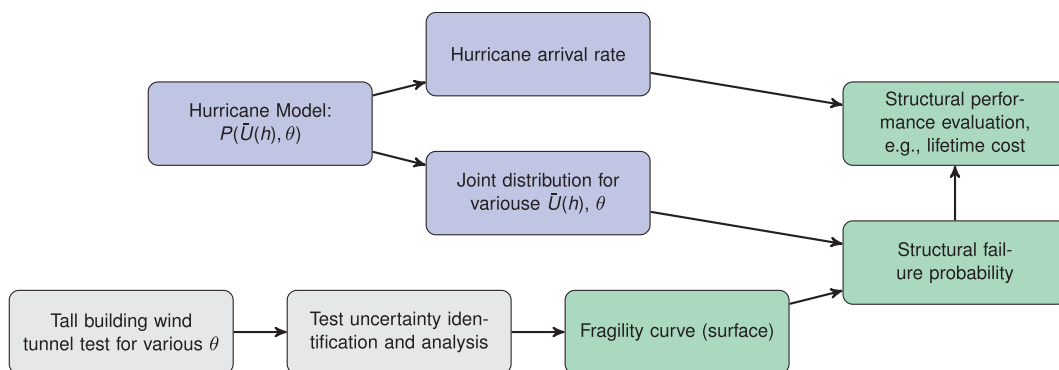


**Fig. 5.** Flow chart of structural PDB framework under wind loads.

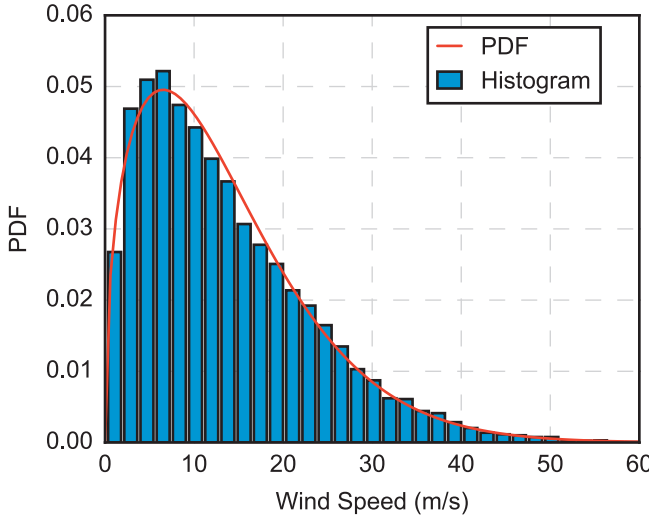


**Fig. 6.** Distribution of hurricane reference (gradient) wind speed at Miami, FL (USA): empirical histogram and PDF model.

Following the procedure described in [62], the variability in the wind force estimated from wind tunnel tests can be synthetically reproduced in accordance with the Monte Carlo simulation method. Consequently, this variability can be transferred to the analysis of the structural dynamic response (Section 3.3.3). As a result, the distribution of a relevant set of structural response parameters (EDP) can be computed by assembling all results from the Monte Carlo simulation. Relevant examples of EDP, used in this study, are: maximum lateral displacement and maximum torsional rotation at the building roof-top.

For the CAARC building, when the reference wind speed  $\bar{U}(h)$  is 25 m/s and the relative mean-wind incidence angle  $\Psi$  is  $0^\circ$ , the distribution of the roof-top maximum displacement is plotted in Fig. 9a. The maximum displacement is the modulus of the resultant displacement, which combines the along-wind direction and cross-wind direction components. Since the resultant displacement is a non-Gaussian process, the translation process theory is used to calculate the modulus of the maximum resultant displacement [24].

Fig. 9b illustrates the distribution of the maximum torsional rotation when the wind speed  $\bar{U}(h)$  is 35 m/s and the relative mean-wind incidence angle  $\Psi$  is  $\pi/2$  ( $90^\circ$ ). Since the torsional rotation, excited by stationary wind speed process can be approx-

imately considered as an independent Gaussian process, the standard method ([70]) is used to determine its maximum value. Furthermore, the limit states associated with maximum roof-top lateral displacement and maximum torsional rotation are plotted in Fig. 9a and b. The threshold for the maximum structural displacement is  $h/400 = 0.46$  m; it is assumed as  $5 \times 10^{-3} = 0.3^\circ$  for the torsional rotation angle.

After combining all the probability results at various wind speeds and directions, the fragility surface of the CAARC building is found in Fig. 10a for the former limit state. Since the wind direction is an angular variable, the fragility surface is plotted using polar coordinates. Because of the symmetrical floor plan of the CAARC building, the fragility surface is only plotted when the relative mean-wind incidence angle is  $0 \leq \Psi \leq \pi/2$ . Examination of Fig. 10a suggests that, apart from the wind speed, the probability of exceeding the specific limit state also depends on the relative wind direction. For intermediate values of the wind speed, the probability determined for relative wind direction  $\Psi = \pi/4$  ( $45^\circ$ ) is lower than the one found for other relative wind directions. This observation confirms the relevance of a comprehensive multidirectional wind load and response analysis.

Similarly, Fig. 10b illustrates the fragility surface of the CAARC building associated with maximum torsional rotation limit state. This fragility surface exhibits large dependency on the relative mean-wind incidence angle. The fragility is 1 when the wind speed  $\bar{U}(h) \geq 35$  m/s and  $\Psi$  is close to  $\pi/2$  ( $90^\circ$ ). For other combinations of wind speed and direction, the fragility rapidly decreases to 0. At  $\Psi = 0^\circ$  the fragility is always 0 for all wind speeds. The reason is that, when the relative mean-flow direction is orthogonal to the short edge of the building ( $\Psi = \pi/2$ ), strong vortex shedding will generate a distributed force directed along the long sides of the building; this load will excite both lateral translation in the x direction and torsion, since the two motion components are coupled.

According to Eq. (16), the structural failure probability associated with the two limit states, maximum lateral displacement and maximum torsional angle, is presented in Fig. 11a and b as a function of the variable building orientation  $\Omega$ . The curves presented in Fig. 11 indicate small dependence of the failure probability on the mean wind direction. However, the accumulated lifetime intervention cost will amplify the directionality effect and induce a non-negligible influence of direction, as later discussed in this section.

In particular, further investigation will suggest that the building orientation can become important; the angle  $\Omega$  will affect

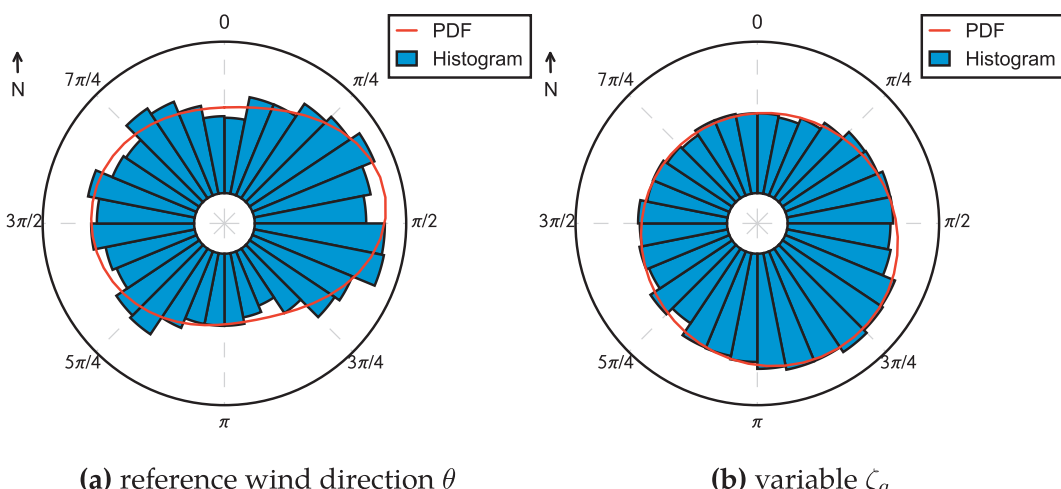


**Fig. 7.** Angular distributions of hurricane reference wind direction  $\theta$  and variable  $\zeta_g$  at Miami, FL (USA): empirical histograms and PDF models.

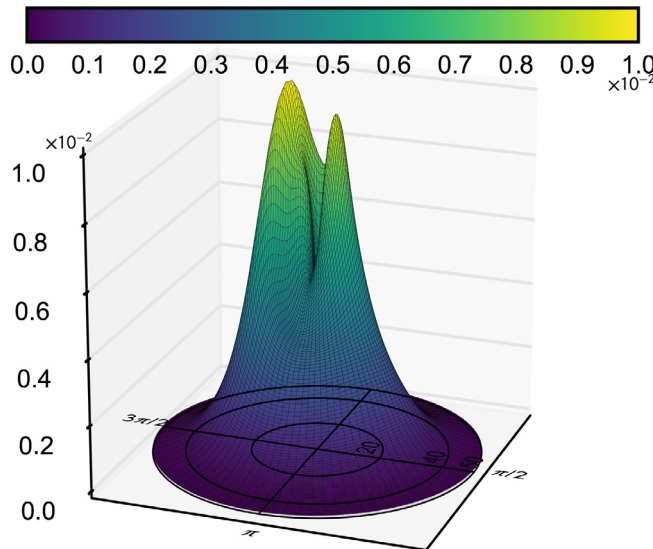


**Fig. 8.** Joint PDF of the gradient wind speed and direction.

structural integrity when lifetime costs are considered because wind climate is clearly direction-dependent. Since the CAARC building floor-plan has two axes of symmetry, the structural failure probability exhibits periodic variations in Fig. 11. For an unsymmetrical building shape, the failure probability will possibly exhibit stronger dependency on the direction  $\Omega$ .

#### 4.3. Lifetime intervention cost analysis: Supplementary verification of the assumptions

The previous information is subsequently combined to examine lifetime intervention cost due to non-structural damage, mainly affecting the cladding components on the building envelope. Damage reports consequent to a hurricane landfall tend to suggest that, in general, wind-induced damage suffered by a high-rise building can usually be associated with non-structural failures in the cladding elements. Strength-related limit states (e.g., large pressure load inducing failures on the cladding or the load-bearing structural systems) are not the main source of damage, in contrast with a low-rise building, in which most damage and repair are dictated by strength of the main structural elements and water intrusion. Damage to glass cladding in the upper floors of a tall buildings,

during high-wind storms, can be related to inter-story drift ratios; supplementary discussion about inter-story drift ratios causing glass cladding damage on building façades can be found, for example, in [71,8]. These observations and the literature review indicate that maximum roof-top displacement and rotations can be used to examine damage, since they are related to inter-story drifts, and justify the use of the two limit states previously defined, with  $l = \{1, 2\}$  being either the roof-top peak lateral displacement or the torsional angle. Even though the limit state associated with wind-borne debris impact may be important in the lower floors of tall buildings (e.g., [72]), it is not considered in this section.

In the absence of explicit protocols for wind load and structural fragility analysis, considering the limit states  $l = \{1, 2\}$  described above, the seismic design guidelines provided by FEMA (Federal Emergency Management Agency) in the United States can be employed [73]. For instance, structural fragility curves associated with "window glass cracking" and "window glass falling from frame", as mandated by FEMA-P-58, can be adapted and included into the structural analysis for wind-induced damage, as investigated in a recent study [29]. In fact, if the dynamic response is dominated by the fundamental modes and flexural mode shapes are described by a linear function of the height  $z$ , the definition of a limit state based on roof-top lateral displacements, given as a fraction of the building height, coincides with the definition of inter-story drift ratio. FEMA-P-58 suggests that, for example, the failure probability (structural fragility) for a standard glass window panel is about 5% in the case of inter-story drift ratios of about 0.01. This value is not incompatible with the limit state  $h/400$  ( $l = 1$ ) employed in this study to accumulate the costs, and consequently provides adequate verification of the proposed approach for the purpose of this study.

Capitalizing from the original formulation adapted from earthquake engineering [27], the intervention cost is taken as a constant percentage of the initial construction cost  $\epsilon_i$ , which depends on the specific limit state  $l = \{1, 2\}$ . Quantification of damage based on a scalar monetary variable applied to the limit states described above is, in fact, correct in the case of a building structure with linear mode shapes and approximate (yet still acceptable) with non-linear mode shape functions. Nevertheless, even though the formulation can accumulate damage costs at the component level, e.g., by independently examining each cladding element on each floor [29] and accounting for inter-story drifts variable with  $z$ , this additional aspect is not considered herein. The main purpose of this section is to demonstrate that the proposed approach can adequately compare various design solutions and use cost projections

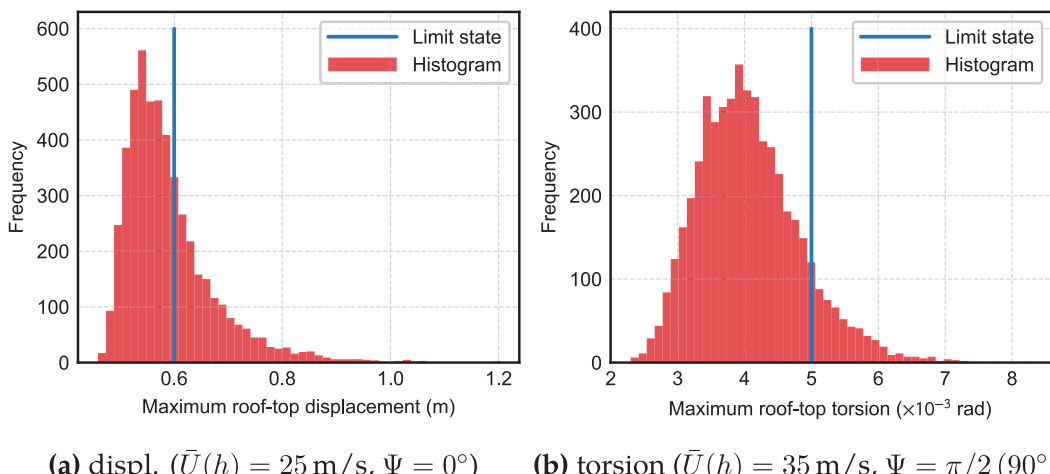


**Fig. 9.** Empirical probability distributions of structural roof-top lateral displacement and torsional angle.

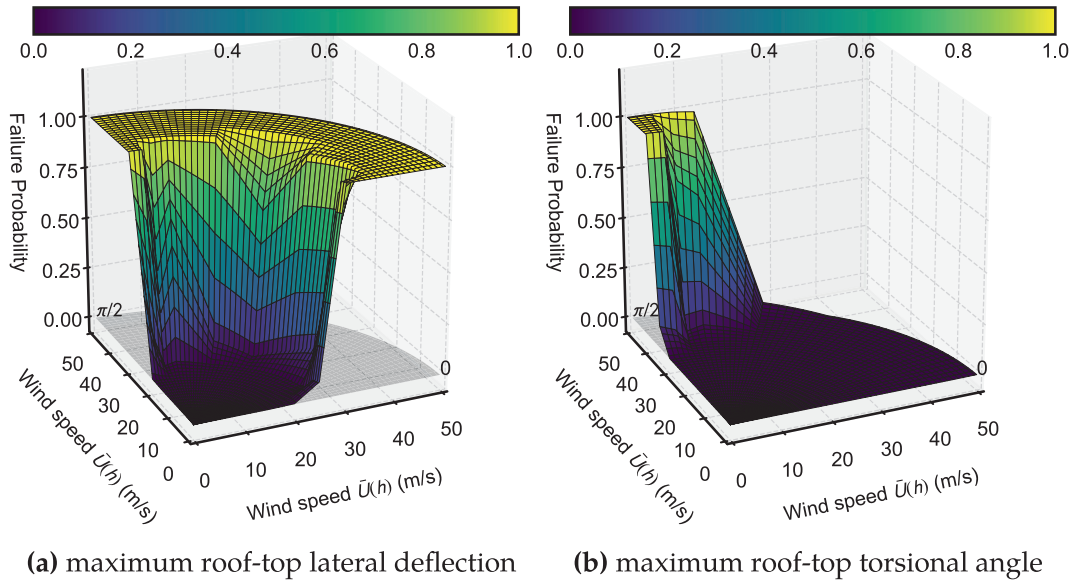


**Fig. 10.** Fragility surfaces of the CAARC building for the limit states of maximum roof-top lateral deflection and maximum roof-top torsional angle.

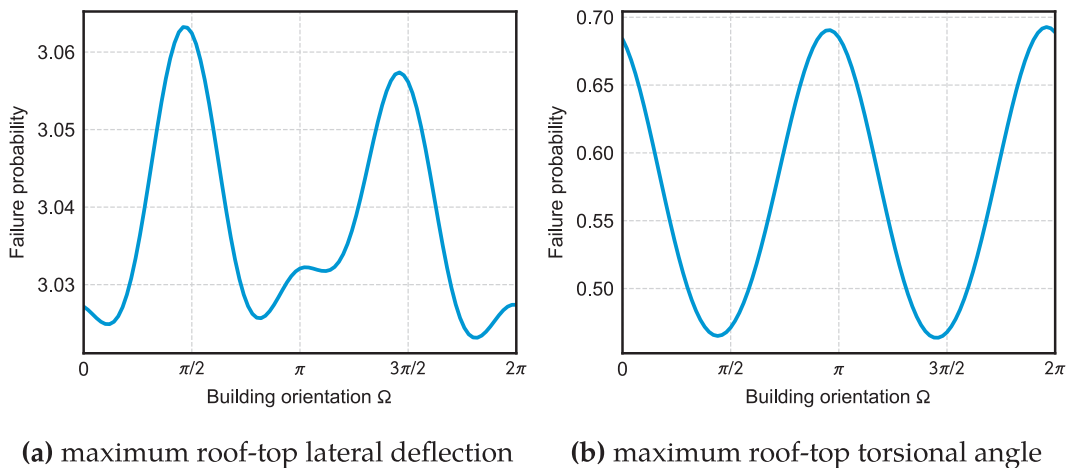


**Fig. 11.** Structural failure probability associated with the limit states of maximum roof-top lateral displacement and maximum roof-top torsional angle.

over structural lifetime to identify an “optimal” configuration, by emphasizing the combined role of maximum wind speed and direction during hurricanes.

#### 4.4. Lifetime intervention cost analysis: Investigation on the effects of wind directionality ( $\Psi$ ) and normalized cost variables ( $\epsilon_l$ )

Structural failure associated with roof-top lateral displacement is initially considered as a minor damage with cost  $\epsilon_1 = 0.02$  (i.e., representing a maintenance needed by cladding components). Failure due to torsional rotation is treated, instead, as a major damage with  $\epsilon_1 = 0.40$  (i.e., simulating the replacement of several cladding elements on the façade). Selection of the two monetary variables for this first cost scenario is compatible with previous studies, carried out using the same building model and configuration [24,45]. Furthermore, a second cost scenario is examined in this subsection to study the effect of the intervention costs, considering  $\epsilon_1$  and  $\epsilon_2$  with the same importance:  $\epsilon_1 = \epsilon_2 = 0.10$ . According to Eq. (18), the structural lifetime intervention cost due to hurricane wind damage is calculated for variable building orientation. Fig. 12a illustrates the maximum lifetime cost for the first normal-

ized cost scenario with  $\epsilon_1 = 0.02$  and  $\epsilon_2 = 0.40$ ; in this case the worst building orientation is found as  $\Omega = 1.96\pi$  ( $353^\circ$ ), which corresponds to the largest structural failure probability; the minimum lifetime cost is achieved with the best building orientation  $\Omega = 1.46\pi$  ( $263^\circ$ ), which is related to the lowest structural failure probability. Fig. 12b illustrates the same aspect for the second cost scenario with  $\epsilon_1 = \epsilon_2 = 0.10$ . In this second case the worst building orientation is found as  $\Omega = 0.48\pi$  ( $86^\circ$ ) and the best building orientation is  $\Omega = 0.18\pi$  ( $32^\circ$ ). The comparison between Fig. 12a and b confirms that the intervention cost predominantly depends on the sensitivity of building damage to the building orientation and the corresponding intervention cost consequent to damage. When the building damage probability is sensitive to the orientation and the intervention cost is large, as for example in the case of the lateral-displacement limit state and the first cost scenario, the building orientation will have a non-negligible impact on the lifetime intervention cost accumulation.

The analysis of both Fig. 12a and b shows that building orientation can ultimately influence structural safety, which is also sensitive to the monetary variables  $\epsilon_1$  and  $\epsilon_2$ . In the case of Fig. 12a and the first cost scenario, non-negligible relative intervention cost

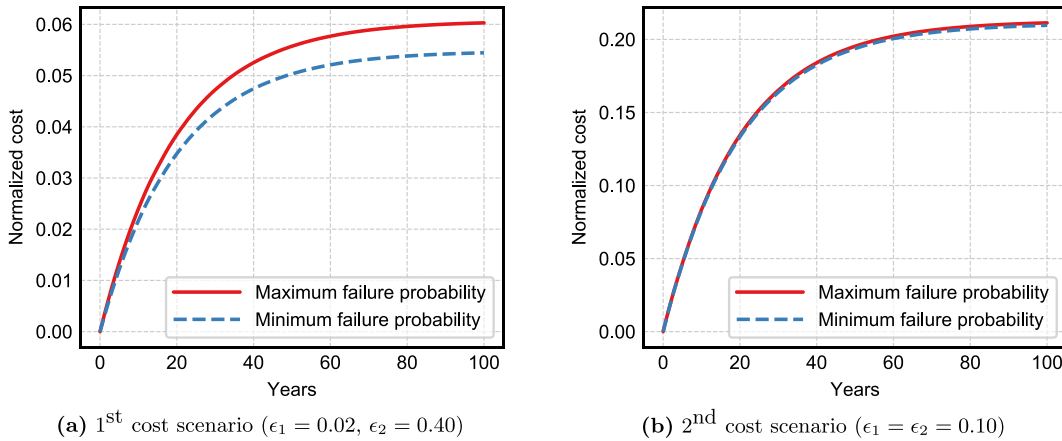


**Fig. 12.** Intervention cost associated with the maximum [worst building orientation] and minimum [best building orientation] structural failure probability.

savings are observed. The cost savings are about 15% (asymptotically) from the examination of the specific application example in Fig. 12a at lifetime  $t = 100$  years. It is also noted that, in spite of the small differences initially observed in Fig. 11, which analyzes one event at a time, the influence of wind directionality can no longer be neglected when lifetime intervention cost accumulation is considered.

Even though the selected  $\epsilon_1$  and  $\epsilon_2$  values may possibly call for a more detailed examination of the cost, for example based on construction management approaches and standardized unit cost estimation, the simulation examples appear adequate for the objectives of this study. More detailed intervention cost evaluation is available for seismic PBD (e.g., [74]); a similar approach could readily be considered in future applications.

## 5. Conclusion

This paper presents a numerical simulation framework for performance-based wind and structural engineering with a focus on hurricane winds and multi-directional aerodynamic loading analysis. The CAARC tall building is the benchmark application. The framework can be separated into sequential modules, which are a “performance-based engineering application” of the Davenport Chain. First, the hurricane simulation method is employed to provide wind climate information and to derive the joint probability distribution of reference wind speed and wind direction. Second, wind tunnel experiments are performed to evaluate multi-directional wind loads along with their experimental errors through a novel probabilistic model. Third, a three-directional structural response model is used to derive the structural fragility surfaces for the tall building. Fragility surfaces are employed to determine structural failure probability (limit states) for various building orientation angles. At last, the structural lifetime intervention cost due the hurricane wind damage is assessed from the failure probability. In summary, this study provides a unified solution to examine the building “failure” probability, considering both wind speed and wind direction, and evaluates structural resilience of tall buildings against hurricane damage in the United States.

## Acknowledgments

This material is based upon work supported in part by the National Science Foundation (NSF) of the United States of America under CAREER grant CMMI-0844977 in 2009–2014. The partial support of NSF grant CMMI-1434880 is also acknowledged. Any

opinions, findings and conclusions or recommendations are those of the authors and do not necessarily reflect the views of the NSF.

## References

- [1] SEAOC. Vision 2000: Performance based seismic engineering of buildings. Sacramento, California: Structural Engineers Association of California; 1995.
- [2] Inokuma A. Basic study of performance-based design in civil engineering. *J Prof Issues Eng Educ Pract* 2002;128(1):30–5.
- [3] Ciampoli M, Petrini F. Performance-based Aeolian risk assessment and reduction for tall buildings. *Probab Eng Mech* 2012;28:75–84.
- [4] Pozzuoli C, Bartoli G, Peil U, Clobes M. Serviceability wind risk assessment of tall buildings including aeroelastic effects. *J Wind Eng Ind Aerodyn* 2013;123 (Part B):325–38.
- [5] Bashor R, Kareem A. Probabilistic performance evaluation of buildings: an occupant comfort perspective. In: Proceedings of the 12th International Conference on Wind Engineering; 2007.
- [6] Bernardini E, Spence S, Gioffrè M, Kareem A. A reliability approach for the wind-induced response assessment of tall buildings using the high frequency force balance. In: The Seventh International Colloquium on Bluff Body Aerodynamics and Applications (BBAAT); 2012, p. 825–834.
- [7] Bernardini E, Spence SM, Kareem A. A Probabilistic approach for the full response estimation of tall buildings with 3d modes using the HFFB. *Struct Saf* 2013;44:91–101.
- [8] Griffis LG. Serviceability limit states under wind load. *Eng J Am Inst Steel Constr* 1993;30:1–16.
- [9] Unanwa C, McDonald J, Mehta K, Smith D. The development of wind damage bands for buildings. *J Wind Eng Ind Aerodyn* 2000;84(1):119–49.
- [10] Chuang WC, Spence SM. A performance-based design framework for the integrated collapse and non-collapse assessment of wind excited buildings. *Eng Struct* 2017;150:746–58.
- [11] Ellingwood B, Rosowsky D, Li Y, Kim J. Fragility assessment of light-frame wood construction subjected to wind and earthquake hazards. *J Struct Eng* 2004;130(12):1921–30.
- [12] Ellingwood B, Tekle P. Wind load statistics for probability-based structural design. *J Struct Eng* 1999;125(4):453–63.
- [13] Li Y, Ellingwood BR. Hurricane damage to residential construction in the US: importance of uncertainty modeling in risk assessment. *Eng Struct* 2006;28 (7):1009–18.
- [14] van de Lindt J, Dao T. Performance-based wind engineering for wood-frame buildings. *J Struct Eng* 2009;135(2):169–77.
- [15] Barbato M, Petrini F, Unnikrishnan VU, Ciampoli M. Performance-based hurricane engineering (PBHE) framework. *Struct Saf* 2013;45:24–35.
- [16] Spence SM, Gioffrè M. Large scale reliability-based design optimization of wind excited tall buildings. *Probab Eng Mech* 2012;28:206–15.
- [17] Spence SM, Kareem A. Performance-based design and optimization of uncertain wind-excited dynamic building systems. *Eng Struct* 2014;78:133–44.
- [18] Seo DW, Caracoglia L. Statistical buffeting response of flexible bridges influenced by errors in aeroelastic loading estimation. *J Wind Eng Ind Aerodyn* 2012;104:129–40.
- [19] Seo DW, Caracoglia L. Estimating life-cycle monetary losses due to wind hazards: Fragility analysis of long-span bridges. *Eng Struct* 2013;56: 1593–606.
- [20] Smith MA. A Monte Carlo based method for the dynamic performance analysis of tall buildings under turbulent wind loading MS Thesis. Boston, Massachusetts, USA: Northeastern University; 2009.
- [21] Cui W, Caracoglia L. New GPU computing algorithm for wind load uncertainty analysis on high-rise systems. *Wind Struct Int J* 2015;21(5):461–87.

- [22] Cui W, Caracoglia L. An efficient physics-based method for eliminating spurious resonant frequencies in high-frequency force balance tests. Porto Alegre, Brazil: Federal University of Rio Grande do Sul; 2015.
- [23] Cui W, Caracoglia L. A Monte-Carlo algorithm for analyzing lifetime maintenance costs on vertical tall structures induced by wind hazards. In: International Conference of the Engineering Mechanics Institute (EMI2014). Hamilton, Ontario, Canada: McMaster University; 2014.
- [24] Cui W, Caracoglia L. Simulation and analysis of intervention costs due to wind-induced damage on tall buildings. Eng Struct 2015;87:183–97.
- [25] Lee JY, Ellingwood BR. Intergenerational risk-informed decision framework for civil infrastructure. In: Deodatis G, Ellingwood BR, Frangopol DM, editors. Safety, Reliability, and Life-Cycle Performance of Structures and Infrastructures. Balkema: CRC Press; 2014. p. 3369–74.
- [26] Lee JY, Ellingwood BR. Impacts of climate change on long-term risk to building structures exposed to hurricanes. American Society of Civil Engineers; 2014.
- [27] Wen YK, Kang YJ. Minimum building lifecycle cost design criteria. I: Methodology. J Struct Eng (ASCE) 2001;127(3):330–7.
- [28] Ierimonti L, Caracoglia L, Venanzi I. Probability-based direct numerical estimation of wind-induced non-structural damage on tall buildings. In: Eighth International Colloquium on Bluff Body Aerodynamics (BBAA VIII). Boston, Massachusetts, USA: Northeastern University; 2016.
- [29] Ierimonti L, Caracoglia L, Venanzi I, Materazzi AL. Investigation on life-cycle damage cost of wind-excited tall buildings considering directionality effects. J Wind Eng Ind Aerodyn 2017;171:207–18.
- [30] Jain A, Srinivasan M, Hart GC. Performance based design extreme wind loads on a tall building. Struct Des Tall Build 2001;10(1):9–26.
- [31] Davenport AG. A statistical approach to the treatment of wind loading on tall masts and suspension bridges Ph.D. Dissertation. United Kingdom: University of Bristol; 1961.
- [32] Isyumov N, Alan G. Davenport's mark on wind engineering. J Wind Eng Ind Aerodyn 2012;104:12–24.
- [33] Piccardo G, Solari G. Closed form prediction of 3-D wind-excited response of slender structures. J Wind Eng Ind Aerodyn 1998;74:697–708.
- [34] Dyrbøe C, Hansen SO. Wind loads on structures. 1st ed. New Jersey, USA: John Wiley & Sons; 1997.
- [35] Davenport AG. The response of supertall buildings to wind. In: Second century of the skyscraper. Springer; 1988. p. 705–25.
- [36] Davenport AG. The response of six building shapes to turbulent wind. Philos Trans R Soc London Ser A, Math Phys Sci 1971;269(1199):385–94.
- [37] Piccardo G, Solari G. Generalized equivalent spectrum technique. Wind Struct 1998;1(2):161–74.
- [38] Kareem A. Acrosswind response of buildings. J Struct Div 1982;108(4):869–87.
- [39] Yi J, Li Q. Wind tunnel and full-scale study of wind effects on a super-tall building. J Fluids Struct 2015;58:236–53.
- [40] Yeo D, Simiu E. High-rise reinforced concrete structures: database-assisted design for wind. J Struct Eng 2011;137(11):1340–9.
- [41] NOAA, National Data Buoy Center, <http://www.ndbc.noaa.gov/>, 2015 [Online; accessed 30-September-2015].
- [42] Vickery PJ, Wadhwa D, Galsworthy J, Peterka JA, Irwin PA, Griffis LA. Ultimate wind load design gust wind speeds in the united states for use in ASCE-7. J Struct Eng (ASCE) 2009;136(5):613–25.
- [43] Vickery P, Skerlj P, Twisdale L. Simulation of hurricane risk in the U.S. using empirical track model. J Struct Eng 2000;126(10):1222–37.
- [44] Vickery PJ, Twisdale LA. Wind-field and filling models for hurricane wind-speed predictions. J Struct Eng 1995;121(11):1700–9.
- [45] Cui W, Caracoglia L. Exploring hurricane wind speed along US Atlantic coast in warming climate and effects on predictions of structural damage and intervention costs. Eng Struct 2016;122:209–25.
- [46] Landsea CW, Hagen A, Bredemeyer W, Carrasco C, Glenn DA, Santiago A, Strahan-Sakoskie D, Dickinson M. A Reanalysis of the 1931–43 Atlantic Hurricane Database. J Clim 2014;27(16):6093–118.
- [47] Georgiou PN. Design wind speeds in tropical cyclone-prone regions Ph.D. Dissertation. London, Ontario, Canada: University of Western Ontario; 1986.
- [48] Lee KH, Rosowsky DV. Synthetic hurricane wind speed records: development of a database for hazard analyses and risk studies. Nat Hazards Rev 2007;8(2):23–34.
- [49] Johnson RA, Wehrly TE. Some angular-linear distributions and related regression models. J Am Stat Assoc 1978;73(363):602–6.
- [50] Carta JA, Ramírez P, Bueno C. A joint probability density function of wind speed and direction for wind energy analysis. Energy Convers Manage 2008;49(6):1309–20.
- [51] Melbourne WH. Comparison of measurements on the CAARC standard tall building model in simulated model wind flows. J Wind Eng Ind Aerodyn 1980;6(1):73–88.
- [52] Tanaka H, Lawen N. Test on the CAARC standard tall building model with a length scale of 1: 1000. J Wind Eng Ind Aerodyn 1986;25(1):15–29.
- [53] Goliger A, Milford R. Sensitivity of the CAARC standard building model to geometric scale and turbulence. J Wind Eng Ind Aerodyn 1988;31(1):105–23.
- [54] Obasaju E. Measurement of forces and base overturning moments on the CAARC tall building model in a simulated atmospheric boundary layer. J Wind Eng Ind Aerodyn 1992;40(2):103–26.
- [55] Tang U, Kwok K. Interference excitation mechanisms on a 3DOF aeroelastic CAARC building model. J Wind Eng Ind Aerodyn 2004;92(14):1299–314.
- [56] Thepmongkorn S, Wood G, Kwok K. Interference effects on wind-induced coupled motion of a tall building. J Wind Eng Ind Aerodyn 2002;90(12):1807–15.
- [57] Huang S, Li Q, Xu S. Numerical evaluation of wind effects on a tall steel building by CFD. J Constr Steel Res 2007;63(5):612–27.
- [58] Braun AL, Awruch AM. Aerodynamic and aeroelastic analyses on the CAARC standard tall building model using numerical simulation. Comput Struct 2009;87(9):564–81.
- [59] Elshaer A, Aboshasha H, Bitsuamlak G, Damatty AE, Dagnew A. LES evaluation of wind-induced responses for an isolated and a surrounded tall building. Eng Struct 2016;115(Supplement C):179–95.
- [60] Smith MA, Caracoglia L. A Monte Carlo based method for the dynamic fragility analysis of tall buildings under turbulent wind loading. Eng Struct 2011;33(2):410–20.
- [61] Caracoglia L. A stochastic model for examining along-wind loading uncertainty and intervention costs due to wind-induced damage on tall buildings. Eng Struct 2014;78:121–32.
- [62] Cui W, Caracoglia L. Examination of experimental variability in HFFB testing of a tall building under multi-directional winds. J Wind Eng Ind Aerodyn 2017;171:34–49.
- [63] Saunders J, Melbourne W. Tall rectangular building response to cross-wind excitation. London: Cambridge University Press; 1975. p. 369–80.
- [64] Holmes J. Mode shape corrections for dynamic response to wind. Eng Struct 1987;9(3):210–2.
- [65] Cui W, Caracoglia L. Physics-based method for the removal of spurious resonant frequencies in High-Frequency Force Balance tests. J Struct Eng, ASCE 2016;142(2):04015129.
- [66] Cui W, Caracoglia L. A fully-coupled generalized model for multi-directional wind loads on tall buildings: A development of the quasi-steady theory. J Fluids Struct 2018;78:52–68.
- [67] Zhou Y, Kareem A, Gu M. Mode shape corrections for wind load effects. J Eng Mech 2002;128(1):15–23.
- [68] Cui W, Caracoglia L. Climate change impact on lifetime monetary losses due to hurricane-induced damage on tall buildings. In: International Conference of the Engineering Mechanics Institute (EMI2015). California, USA: Stanford University; 2015.
- [69] Batts ME, Simiu E, Russell LR. Hurricane wind speeds in the United States. J Struct Div 1980;106(10):2001–16.
- [70] Davenport AG. Note on the distribution of the largest value of a random function with application to gust loading. In: ICE Proceedings. Thomas Telford; 1964. p. 187–96.
- [71] AAMA. Recommended static test method for evaluating curtain wall and storefront systems subjected to seismic and wind induced interstory drifts (501.4) and recommended dynamic test method for determining the seismic drift causing fallout from a wall system (501.6). Schaumburg, Illinois, USA: American Architectural Manufacturers Association (AAMA); 2009.
- [72] Moghim F, Caracoglia L. A numerical model for wind-borne compact debris trajectory estimation: part 1 – probabilistic analysis of trajectory in the proximity of tall buildings. Eng Struct 2012;38:153–62.
- [73] FEMA-P-58, Seismic performance assessment of building, volume 3, Technical report (<http://www.fema.gov/media-library/assets/documents/90380>), Federal Emergency Management Agency, United States, 2012.
- [74] Ramirez C, Liel AB, Mitrani-Reiser J, Haselton CB, Spear AD, Steiner J, et al. Expected earthquake damage and repair costs in reinforced concrete frame buildings. Earthquake Eng Struct Dynam 2012;41(11):1455–75.